







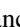








The MOSDEF Survey: Stellar Continuum Spectra and Star Formation Histories of Active, Transitional, and Quiescent Galaxies at $1.4 < z < 2.6$

Tom O. Zick^{1,2}, Mariska Kriek¹ , Alice E. Shapley³ , Naveen A. Reddy⁴ , William R. Freeman⁴ , Brian Siana⁴ , Alison L. Coil⁵ , Mojegan Azadi⁶ , Guillermo Barro⁷ , Tara Fetherolf⁴, Francesca M. Fornasini⁵ , Laura de Groot⁸, Gene Leung⁷ , Bahram Mobasher⁴, Sedona H. Price⁹ , Ryan L. Sanders³ , and Irene Shivaei¹⁰ 

¹ Astronomy Department, University of California, Berkeley, CA 94720, USA; tzick@berkeley.edu

² Lawrence Livermore National Laboratory, P.O. Box 808 L-210, Livermore, CA 94551, USA

³ Department of Physics & Astronomy, University of California, Los Angeles, 430 Portola Plaza, Los Angeles, CA 90095, USA

⁴ Department of Physics & Astronomy, University of California, Riverside, 900 University Avenue, Riverside, CA 92521, USA

⁵ Center for Astrophysics and Space Sciences, University of California, San Diego, 9500 Gilman Drive, La Jolla, CA 92093-0424, USA

⁶ Harvard-Smithsonian Center for Astrophysics, 60 Garden Street, Cambridge, MA 02138, USA

⁷ Department of Physics, University of the Pacific, 3601 Pacific Avenue, Stockton, CA 95211, USA

⁸ Department of Physics, The College of Wooster, 1189 Beall Avenue, Wooster, OH 44691, USA

⁹ Max-Planck-Institut für extraterrestrische Physik, Postfach 1312, Garching, D-85741, Germany

¹⁰ Department of Astronomy/Steward Observatory, 933 North Cherry Avenue, Room N204, Tucson, AZ 85721-0065, USA

Received 2018 July 20; revised 2018 October 12; accepted 2018 October 12; published 2018 October 30

Abstract

Using the MOSFIRE Deep Evolution Field (MOSDEF) rest-frame optical spectroscopic survey, we investigate the star formation histories (SFHs) of different galaxy types, ranging from actively star-forming to quiescent at $1.4 \leq z \leq 2.6$. SFHs are constrained utilizing stellar continuum spectroscopy, specifically through a combination of Balmer absorption lines, the 4000 Å break, and the equivalent width of the H α emission line. To attain a sufficiently high signal-to-noise ratio (S/N) to conduct these measurements we stack spectra of galaxies with similar spectral types, as determined from their rest-frame $U - V$ and $V - J$ colors. We bin the MOSDEF sample into five spectral types, subdividing the quiescent and star-forming bins to better explore galaxies transitioning between the two. We constrain the average SFHs for each type, finding that quiescent and transitional galaxies in the MOSDEF sample are dominated by an SFH with an average star formation timescale of $\tau \sim 0.1\text{--}0.2$ Gyr. These findings contrast with measurements from the low-redshift Universe where, on average, galaxies form their stars over a more extended time period ($\tau > 1$ Gyr). Furthermore, our spectral index measurements correlate with mass surface density for all spectral types. Finally, we compare the average properties of the galaxies in our transitional bins to investigate possible paths to quiescence, and speculate on the viability of a dusty post-starburst phase.

Key words: galaxies: evolution – galaxies: high-redshift

1. Introduction

A bimodal distribution of galaxy properties (e.g., color, age, morphology) has been observed both in the local universe (e.g., Kauffmann et al. 2003) and up to high redshift (e.g., Williams et al. 2009; Whitaker et al. 2011), defining a red quiescent sequence and a star-forming sequence in color–mass or color–color space. Though a red sequence has been observed out to $z = 3$, the relative abundance of quiescent and star-forming galaxies changes across cosmic time; at low redshifts higher mass galaxies are predominantly quiescent, whereas at $z \geq 2.5$ star-forming galaxies dominate at all masses (e.g., Muzzin et al. 2013; Tomczak et al. 2014). However, the process by which these star-forming galaxies quench and join the quiescent sequence remains poorly understood.

Understanding the evolution of galaxies from star-forming to quiescent requires detailed knowledge of star formation histories (SFHs) for a large, representative population of galaxies. While these measurements are readily available at $z \leq 0.1$ (Kauffmann et al. 2003) and have recently been extended to $z \sim 0.8$ (Wu et al. 2018), the vast majority of quiescent galaxies quench at $z > 1$ (e.g., Muzzin et al. 2013). Therefore, understanding quenching requires pushing studies to even higher redshifts.

Past work around this peak quenching epoch has relied heavily on deep multiwavelength photometry, which yields poor constraints on SFHs due to model degeneracy, lack of spectroscopic detail, and imprecise redshifts. More robust SFHs can be obtained from the stellar continuum by comparing features sensitive to recent star formation, like the Balmer absorption-line index, $H\delta_A$, with features sensitive to age, like the 4000 Å break (D_n4000). Such measurements require high signal-to-noise (S/N) spectroscopy which has in the past only been attained for the brightest, most massive high-redshift sources (e.g., Kriek et al. 2009, 2016; van de Sande et al. 2013; Belli et al. 2015; Barro et al. 2016). Alternatively, one can stack multiple like galaxies to reach a sufficient S/N for characterizing absorption features (Onodera et al. 2012; Mendel et al. 2015); however, such studies have also been conducted primarily for massive quiescent galaxies.

With the recently completed MOSFIRE Deep Evolution Field (MOSDEF) survey (Kriek et al. 2015), in which MOSFIRE spectroscopy was collected for ~ 1500 galaxies at $1.37 \leq z \leq 3.80$, it is now possible to spectroscopically probe the SFHs of a representative high-redshift galaxy population for the first time. In this Letter we present a technique for constructing composite spectra that conserves stellar continuum, enabling us to measure absorption features sensitive to age and short-term

variation in star formation at $z \sim 2$. With this methodology, we characterize SFHs for stacks of galaxies across rest-frame $U - V$ versus $V - J$ color-color space.

Throughout this work we utilize a Chabrier (2003) initial mass function and a Λ CDM cosmology with $\Omega_M = 0.3$, $\Omega_\Lambda = 0.7$ and $H_0 = 70 \text{ km s}^{-1} \text{ Mpc}^{-1}$.

2. Data and Galaxy Sample

This work leverages the full MOSDEF sample, consisting of rest-frame optical (flux-calibrated) spectra for 1493 H-band selected galaxies between $1.37 \leq z \leq 3.80$, with masses and star formation rates (SFRs) ranging from $\sim 10^9 - 10^{11.5} M_\odot$ and $\sim 10^0 - 10^3 M_\odot \text{ yr}^{-1}$, respectively. All MOSDEF galaxies are covered by deep *Hubble Space Telescope* (HST)/WFC3 imaging from CANDELS (Koekemoer et al. 2011; Grogin et al. 2011). For information about target selection, data reduction, and sample parameters see Kriek et al. (2015). For the current work we have selected galaxies with a MOSDEF redshift of $1.37 \leq z \leq 2.61$, as higher redshift galaxies do not typically have sufficient S/N for stacking continuum spectra. We also require at least 400 pixels of coverage within the $3700 \text{ \AA} \leq \lambda \leq 6600 \text{ \AA}$ bandpass, which ensures the validity of our stacking method.

For all 806 spectra in our sample we have measured stellar masses and rest-frame colors using the photometric catalogs constructed by the 3D-HST collaboration (Skelton et al. 2014; Momcheva et al. 2016) in conjunction with MOSDEF redshifts. Masses are obtained by fitting a galaxy's spectral energy distribution (SED) with stellar population synthesis (SPS) models, utilizing the SPS fitting code FAST (Kriek et al. 2009) along with flexible SPS models (FSPS; Conroy et al. 2009), and the Calzetti et al. (2000) attenuation curve. We derive rest-frame colors using EAZY (Brammer et al. 2008) and adopt sizes as measured by van der Wel et al. (2012, 2014) from the CANDELS/F160W photometric band using GalFit and Galapagos (Peng et al. 2002; Barden et al. 2012). We use the circularized r_e from these size measurements to derive the mass surface density (Σ) for each of our galaxies.

3. Stacking MOSDEF Spectra

In this work we bin galaxies by similarity in spectral type as determined by their rest-frame $U - V$ versus $V - J$ colors to attain sufficient S/N per stack to measure SFHs. In the UVJ diagram, dust extinction (A_v) increases linearly with increasing $U - V$ and $V - J$, while specific star formation (sSFR) decreases in an almost perpendicular direction for star-forming galaxies. Once a galaxy has stopped forming stars, it will move along the red sequence as it ages (e.g., Wuyts et al. 2009; Whitaker et al. 2012; Fumagalli et al. 2014; Yano et al. 2016). Though galaxies on the quiescent sequence can also be reddened due to increased metallicity, this effect is subdominant to age (Whitaker et al. 2013). We take advantage of these trends in sSFR, age, and dust to bin galaxies as shown in panel (a) of Figure 1. We use the age gradient in the red sequence to separate our post-starburst (ii) from our quiescent bin (i), and split our star-forming sequence into non-dusty star-forming (v), dusty star-forming (iv), and dusty galaxies with lower sSFRs (iii). We show the bin break down of our selected galaxies in color-mass space in Figure 1.

For each bin in UVJ space we generate a composite spectrum from individual spectra with varying wavelength coverage. First, we calculate the average best-fit SPS model in luminosity

density units for each UVJ bin by averaging the best-fit SPS model per member galaxy.

Next, for each individual spectrum, we create a skyline mask ($m_{i,x}$) using an S/N cutoff and interpolate the reduced rest-frame spectrum and mask onto a 0.5 \AA separated grid to approximate the spectral sampling of MOSFIRE. We derive a scaling parameter (s_x) for each individual spectrum using the average best-fit model corresponding to its UVJ bin according to

$$s_x = \frac{\sum_{i=0}^P \omega_{i,x} r_{i,x} m_{i,x}}{\sum_{i=0}^P \omega_{i,x} f_{i,x} m_{i,x}}, \quad (1)$$

where P is the total number of pixels in the spectrum, $f_{i,x}$ is the flux of the i th pixel of a given spectrum x , $\omega_{i,x}$ is its corresponding inverse variance, and $r_{i,x}$ is the corresponding luminosity density of the average best-fit SPS model for each bin.

Finally, we stack each spectrum in a given UVJ bin according to an S/N weighted mean stacking method described by

$$t_i = \frac{\sum_{x=0}^N w_x s_x f_{i,x} m_{i,x}}{\sum_{x=0}^N w_x m_{i,x}}, \quad (2)$$

where t_i is the final stacked value at each pixel and w_x is the average S/N per spectrum.

By scaling spectra to the average best-fit model for their bin, we correct for flux variations due to redshift differences in our sample and mitigate relative calibration issues between bands for a given galaxy.

In Figure 2, we show the resulting composite spectrum and SED for each bin in UVJ space arranged by increasing UV emission relative to the flux at rest-frame 5000 \AA . In Figure 3 we zoom in on the region around $H\alpha$ and $H\delta$ for each of the stacks.

4. Measuring Spectral Features

To measure spectral features for each type, we first mask emission lines from the stacked spectra, then fit them using FAST with high-resolution Bruzual & Charlot (2003) models. In order to determine the $H\alpha$ emission equivalent width (EW ($H\alpha$)), we fit with a triple Gaussian to account for potential contamination by the neighboring [N II] lines, while correcting for underlying stellar absorption using the best-fit SPS model to the spectrum. We do not apply an additional dust correction to the EW($H\alpha$) measurements to account for the possibility of increased extinction toward H II regions, thus they may be underestimated. We remove active galactic nuclei (AGN) from our sample for measurements of $H\alpha$ (see Azadi et al. 2017). Next, we simultaneously fit the other Balmer lines in the raw stacks for absorption and emission, fixing the latter to our measured $H\alpha$ line widths. As can be seen in panel (v) of Figure 2, the emission line widths are considerably narrower than the (pressure broadened) underlying Balmer absorption lines. Given these differing line widths, we can robustly disentangle the emission from the absorption lines. Finally, we use our emission line fit to subtract the emission lines from the spectrum and refit our stacks to measure best-fit star formation timescales.

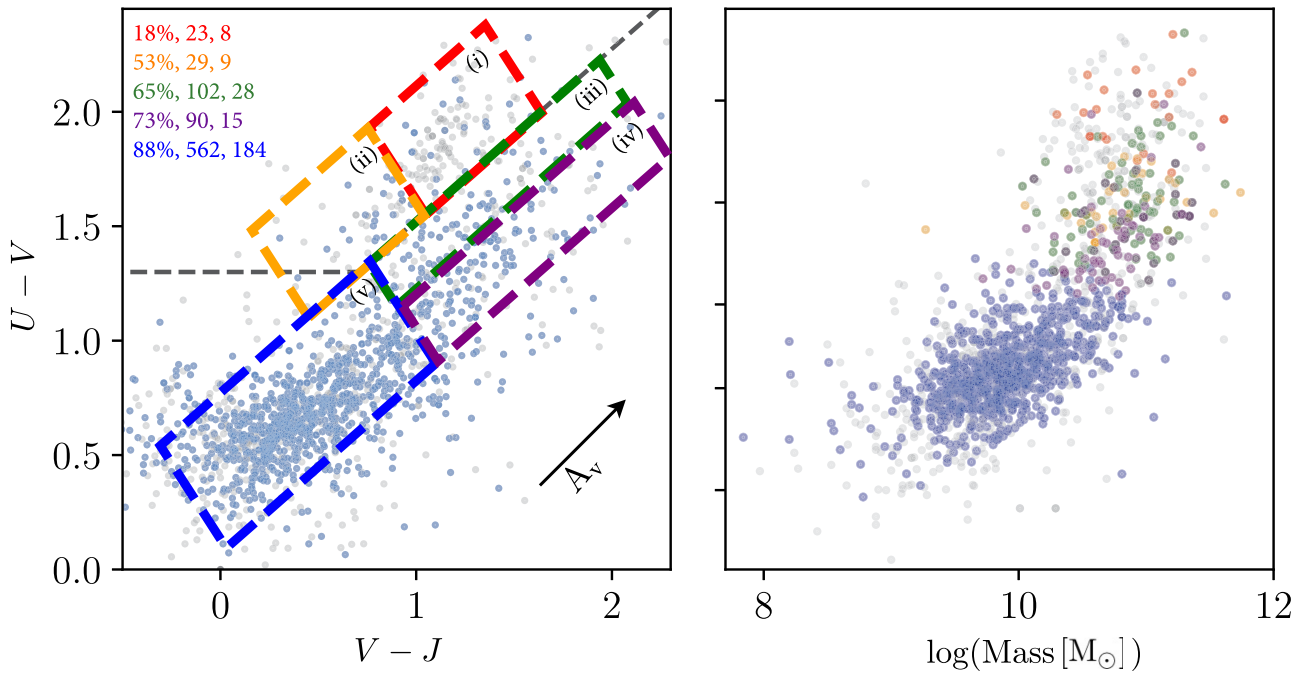


Figure 1. Left: full MOSDEF sample (gray) and our selected sample (blue) in UVJ space, where each box color corresponds to a distinct typical SED shape. On the top left we detail the percent of targets with MOSDEF redshift measurements, the number of spectra with a MOSDEF redshift, and the average number of galaxies per pixel in our composite spectra, colored by corresponding bin. Right: $U - V$ color vs. stellar mass for galaxies (colored by bin) that comprise each stack.

We measure continuum features from the emission-line subtracted stacked spectra, adopting the bandpasses for $H\delta_A$ and D_n4000 described in Worthey & Ottaviani (1997) and Balogh et al. (1999), respectively (see Table 1). The one exception is the post-starburst stack (ii), where the blue continuum bandpass does not consist of sufficient galaxies to reliably measure $H\delta_A$ and we instead measure continuum from the best-fit SPS model to the spectrum.

We derive measurement errors by randomly generating a spectrum, drawing from the noise spectrum of each stack, and repeating our measurements 10,000 times. We take the standard deviation of these measurements as our error. We also test for the sensitivity of each bin to its components by repeating our continuum measurements for stacks with a random $\sim 10\%$ of each bin removed. Our measurement errors exceed the resulting variation for all but the quiescent stack, which is dominated by two especially massive galaxies. We therefore adopt the standard deviation of the bootstrapped ensemble for the quiescent bin measurements.

5. SFH of $z \sim 2$ Galaxies across UVJ Space

We use the spectral features measured in the previous section to infer SFHs for a diverse galaxy population and provide unique insights into galaxy evolution at $z \sim 2$. In both Figures 2 and 3 we see clear trends in spectroscopic properties with increasing UV emission relative to rest-frame optical. To assess these trends, we compare $H\delta_A$, D_n4000 , and $EW(H\alpha)$ measured from our stacks in Figure 4. In panel (a) we compare $H\delta_A$ with D_n4000 . The former peaks when A-type stars dominate the spectrum, which only occurs when a relatively short star formation period is followed by rapid quenching. The latter is sensitive to the opacity of stellar atmospheres and increases with age and metallicity. Comparing the two parameters allows us to assess the evolutionary phase and star formation timescale of a given galaxy (Kauffmann et al. 2003).

Panel (b) compares $H\delta_A$ to $EW(H\alpha)$, another SFH probe that measures the relative importance of $H\alpha$ emission to the underlying stellar continuum. As continuum emission is a proxy for mass and $H\alpha$ arises from recombination around hot and massive O and early B-type stars with short lifetimes, $EW(H\alpha)$ relates star formation within the past 50 Myr to past star formation.

We find that our measurements for the transitional (ii and iii) and quiescent (i) bins form a sequence in both $H\delta_A/D_n4000$ space and $EW(H\alpha)/H\delta_A$ space. These bins are most consistent with a rapid star formation model ($\tau = 0.1\text{--}0.2$ Gyr) shown in panels (a) and (b) of Figure 4 and are therefore most compatible with a fast-quenching SFH. We find consistent results from our best-fit SPS models (see Table 1). Additionally, one of our contributing quiescent galaxies has an independent measurement of $\tau \sim 200$ Myr from $[\alpha/Fe]$ (Kriek et al. 2016), supporting our measurement. The average SFHs of the galaxies in the dusty (iv) and less-obscured (v) star-forming bins are consistent with a more extended star formation timescale (i.e., delayed τ model with $\tau \approx 0.2\text{--}1$ Gyr). This result supports past work finding constant or rising SFHs for star-forming galaxies at $z = 2$ (e.g., Lee et al. 2010; Maraston et al. 2010; Reddy et al. 2012).

We compare our measurements to values from the Max Planck Institute for Astrophysics/Johns Hopkins University (MPA/JHU) Sloan Digital Sky Survey (SDSS) catalogs (Kauffmann et al. 2003; Brinchmann et al. 2004) and find an offset between our transitional and quiescent galaxy bins relative to the median sequence at low redshifts. The inferred star formation timescales in these bins are shorter than for a typical SDSS galaxy ($\tau \geq 1$ Gyr) at the 4σ level, for all but bin (ii), which is significant to 2σ . This offset is expected, as galaxies in the $z \sim 0.1$ universe had a longer period over which stars could have been formed. Nonetheless, the timescales of the transitional galaxies at $z \sim 2$ are substantially shorter than the age of the universe at that time. The Lega-C survey also

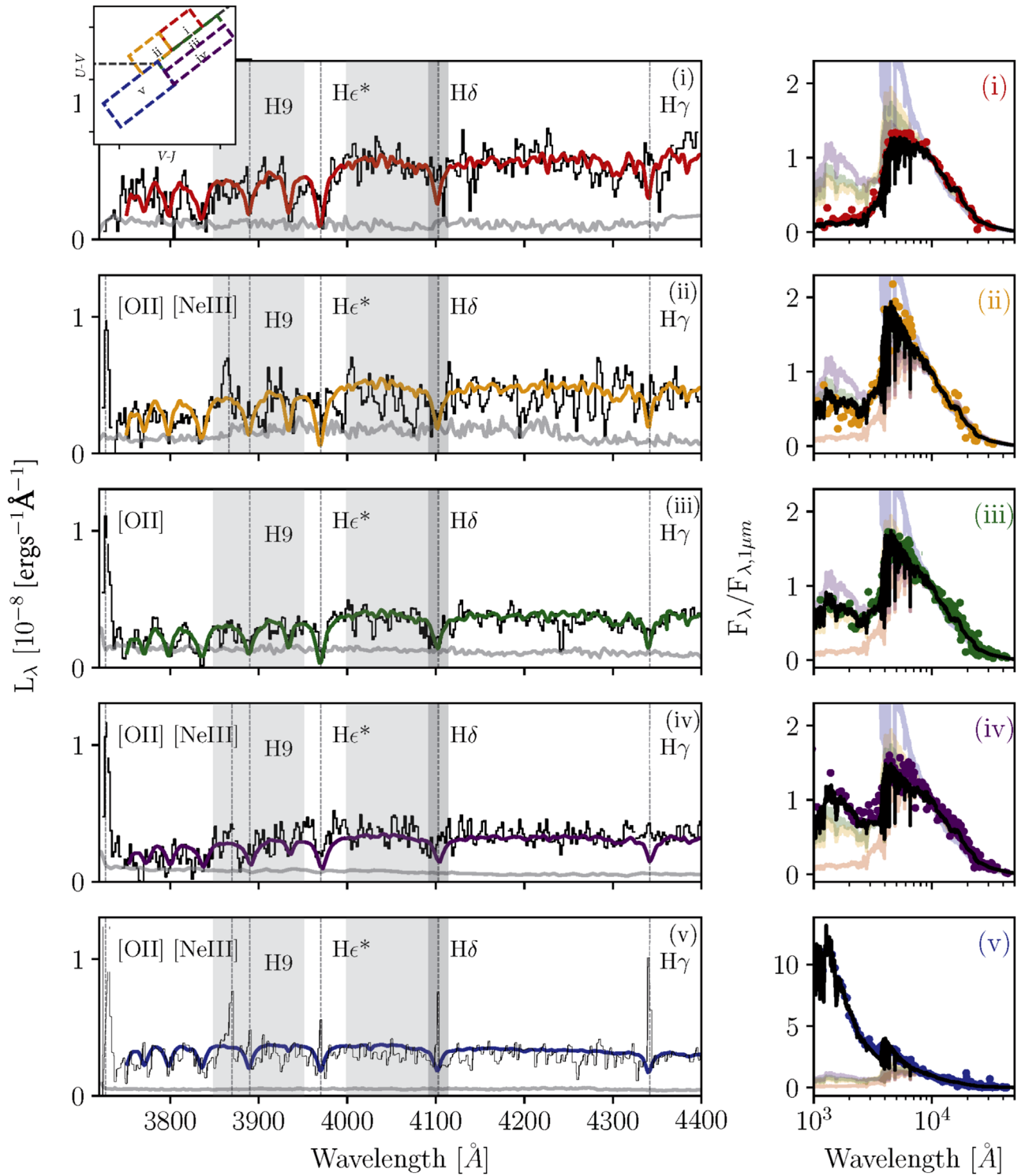


Figure 2. Left: stacked spectra for galaxies binned in UVJ space and ordered by rest-frame UV emission relative to $1 \mu\text{m}$. Each stack (black) and composite noise spectrum (gray) is shown median binned by 2.5 \AA . The colored lines are the FAST fits to the stacked spectra. The bandpasses from which we measure D_n4000 and $H\delta_A$ are shown in gray and dark gray respectively. Right: composite SEDs for each UVJ bin. The colored circles correspond to binned photometric measurements, the black line shows the best fit to the composite SED, while the best fits for the other bins are plotted according to their respective bin color.

finds an offset at $z = 0.8$ for D_n4000 versus $H\delta_A$ measured from individual spectra (Wu et al. 2018). However, as shown in Figure 4, it is less pronounced than for our stacks, implying shorter star formation timescales with increasing redshift.

Past work has shown that quiescent galaxies have a higher mass surface density (Σ) than star-forming ones (e.g., Barro et al. 2014; van Dokkum et al. 2015). Mass has also been found

to correlate with D_n4000 but to a lesser extent (e.g., Kauffmann et al. 2003). As our sample is incomplete in mass in the quiescent region of UVJ space, but Σ is approximately constant within an SED type, we only examine the latter parameter in this work. Using our subdivided blue star-forming and red quiescent bins we assess how Σ varies with spectral type. In Figures 4(c) and (d), we show $\text{EW}(H\alpha)$ and D_n4000 as a

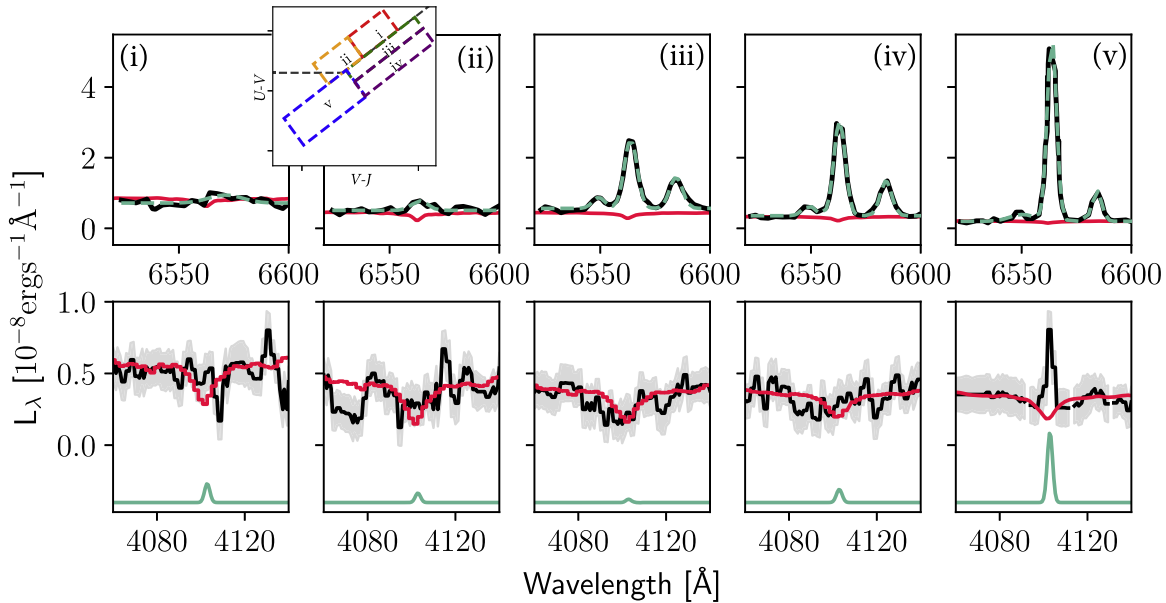


Figure 3. Top: $H\alpha$ region for each stacked spectrum (black). The triple Gaussian fit for the spectra is shown in the dashed teal lines, the best-fit FAST model is shown in red. Bottom: zoom in of the $H\delta_A$ region, with the best fit for the absorption shown in red and the best fit for the emission (fixed to the $H\alpha$ width), shown in teal. The noise spectrum is also plotted (gray). The emission $H\delta$ in (i) is most likely due to AGN activity, as we only remove AGN from our EW($H\alpha$) measurements.

Table 1

Spectral Index Measurements for Each of Our Stacks along with the Best-fit τ from Our FAST Fit (SFH of the Form $SFR(t) \propto te^{-t/\tau}$)

Bin	Log τ (Years)	$H\delta_A$ (Å)	D_n4000	EW($H\alpha$) (Å)
i	8.2	4.9 ± 1.1	1.44 ± 0.05	1 ± 15
ii	8.4	6.2 ± 3.0	1.35 ± 0.10	8 ± 25
iii	8.2	8.4 ± 0.4	1.29 ± 0.09	33 ± 15
iv	9.3	6.3 ± 0.2	1.24 ± 0.09	56 ± 10
v	9.5	7.5 ± 1.3	1.14 ± 0.04	186 ± 19

Note. Each bin number corresponds to the UVJ box as shown in Figure 1.

function of Σ for each of our stacks. We find that EW($H\alpha$) decreases with increasing Σ , which—due to the relative uniformity of mass in all galaxies but those in region (v) of Figure 1—is likely primarily due to decreasing SFR with Σ and not increasing stellar continuum. We also find that D_n4000 increases as a function of Σ . Taken together, these trends motivate a correlation between decreasing sSFR, increasing age, and Σ . This relation may be causal as suggested in van Dokkum et al. (2015), or driven by some alternate physical mechanism with which both parameters are correlated (Lilly & Carollo 2016). Furthermore, as halos, and by extension star formation, which were denser at early times, this sequence could simply be a consequence of the different times at which each of our bins formed their stellar populations with respect to the age of the universe (e.g., Khochfar & Silk 2006; Abramson & Morishita 2018).

Interestingly, a comparison of our composite spectra and measurements for bins (ii) and (iii) in Figure 1 implies that these regions contain related stellar populations. Box (ii) corresponds to galaxies characterized by a recent rapid burst of star formation (e.g., Whitaker et al. 2012; Wild et al. 2016) while box (iii) corresponds to what are usually considered to be dusty star-forming galaxies (e.g., Spitler et al. 2014). However, the similarity in D_n4000 and $H\delta_A$ indicates that both regions are

comparable in age and have stellar populations dominated by a recent burst of star formation. Comparing EW($H\alpha$) to $H\delta_A$ measurements for (iii) indicates suppressed SFR relative to the rapid past star formation that set $H\delta_A$. Additionally, galaxies in region (iii) are dusty, with $E(B - V) = 0.41$ derived from the Balmer decrement as described in Reddy et al. (2015). The characteristics of region (iii) galaxies described above, lead us to speculate that these may be dusty post-starburst galaxies that have not yet expelled or depleted their gas and dust reservoirs (Poggianti et al. 2009). In this picture, the galaxies in region (iii) could be the progenitors of galaxies found in region (ii) at later times.

The short star formation timescale we measure for typical galaxies in region (iii) is inconsistent with the picture of a gradual quenching route to quiescence for our redshift range. This result is in contrast with Belli et al. (2015), who examine spectral fitting derived ages and sizes within the quiescent box and suggest that the galaxies found in our region (iii) may be progenitors of quiescent galaxies that formed their stellar population over an extended time period, skipping the post-starburst phase all together. It is unclear how to reconcile these results, but the tension may be primarily due to the differing redshift regimes probed in each work; the current study targets slightly higher redshifts. Further measurements may be necessary to understand these discrepancies.

6. Discussion

In this Letter we constrain SFH as a function of spectral type for a sample of 806 galaxies from the MOSDEF survey at $1.4 \leq z \leq 2.6$. In order to attain the S/N necessary to constrain SFH from stellar continuum features, we bin galaxies based off of physical trends in $U - V$ versus $V - J$ and utilize a weighted composite stacking method. We find that transitional and quenched galaxies at $z \sim 2$ have a higher $H\delta_A$ for a given D_n4000 than $z \leq 0.8$ galaxies. Specifically, our $z \sim 2$ galaxies are consistent with shorter star formation timescales (100–200 Myr) as compared to $z < 0.8$ (≥ 1 Gyr). We find a

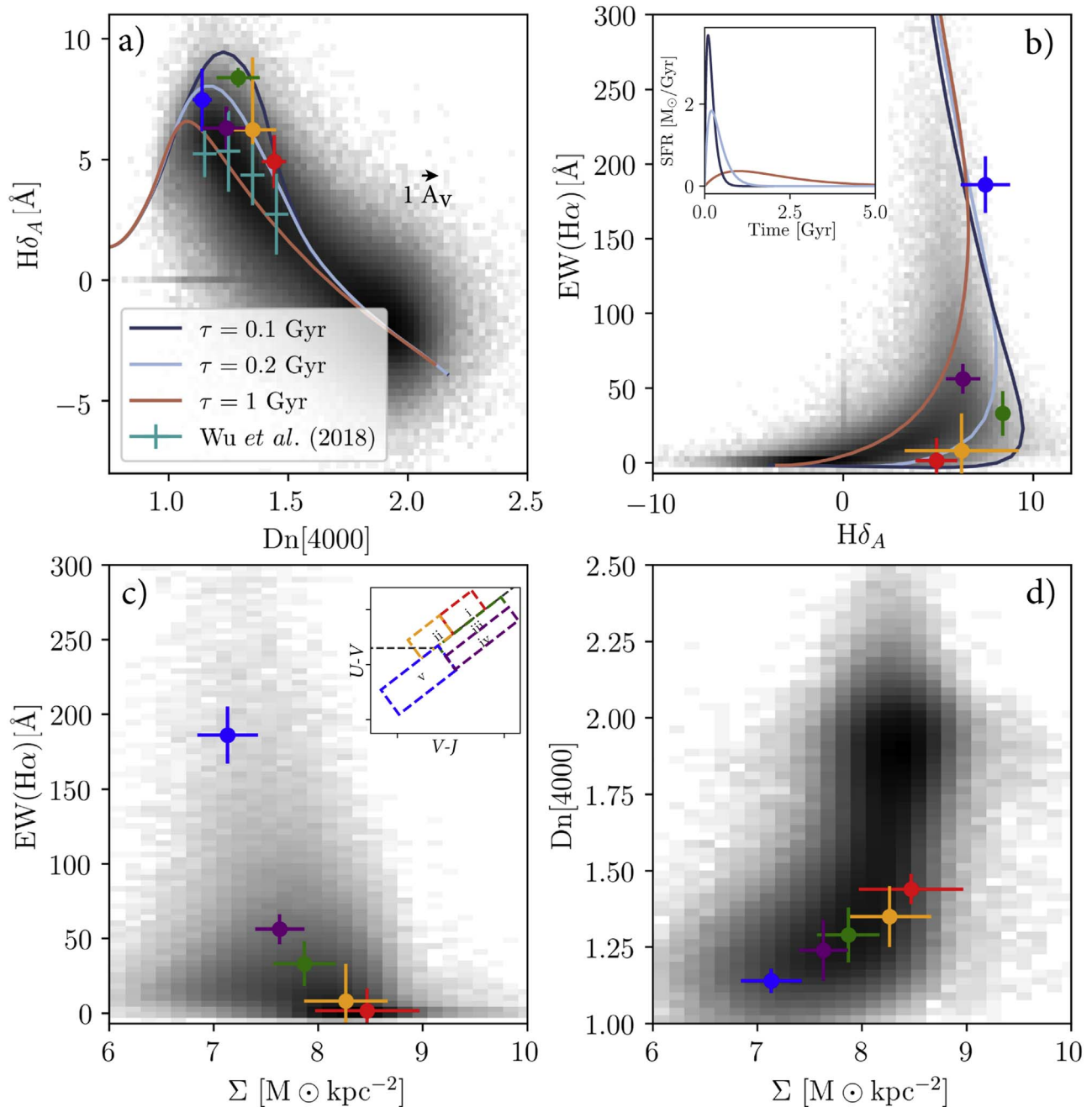


Figure 4. $H\delta_A$, D_n4000 , $EW(H\alpha)$, and Σ measurements for our stacks at $z \sim 2$ colored by their respective UVJ bin, compared to low-redshift values from the SDSS, shown in grayscale. Where applicable, we overplot the FSPS model tracks for three delayed exponential SFHs with $\tau = 0.1, 0.2, 1.0$ Gyr, finding higher $H\delta_A$ than at low redshift for fixed values of D_n4000 . We also show the $z = 0.8$ Wu et al. (2018) distribution where the error bars in D_n4000 and $H\delta_A$ correspond to bin size and standard deviation of the distribution, respectively. As our D_n4000 measurements are not corrected for reddening, we illustrate the effect of $1 A_V$ of extinction with an arrow. Panel (b): $EW(H\alpha)$ vs. $H\delta_A$ measurements confirming that the star formation timescales of transitional galaxies are most consistent with a short $\tau = 100\text{--}200$ Myr SFHs. Panels (c)–(d): $EW(H\alpha)$ and D_n4000 vs. Σ , illustrating a sequence in decreasing $EW(H\alpha)$ and increasing D_n4000 as a function of Σ . Error bars in Σ correspond to the standard deviation of the galaxy ensemble in each bin.

sequence in (increasing) D_n4000 and (decreasing) $EW(H\alpha)$ with Σ , highlighting a relationship between evolutionary phase and Σ , whether it be causal or due to mutual correlation with some third physical parameter. Lastly similarities between the age and SFH of what is usually thought of as part of the dusty star-forming region of the UVJ diagram, to the post-starburst values, motivates that the former may be dusty post-starburst galaxies.














The unique MOSDEF data set enabled several improvements compared to past studies. Most importantly, it increased the

range of galaxy types for which we could constrain stellar populations and SFHs from stellar continuum spectroscopy, ranging from star-forming to transitional to quiescent. Past studies at $z \sim 2$ encompassing the full range of galaxy types focused solely on photometric data, while spectroscopic studies based on stellar continuum at comparable redshifts focused on massive quiescent galaxies. Furthermore, stacking galaxies without subtracting a polynomial fit to the continuum as done in previous works, allows us to measure D_n4000 for a statistical sample of galaxies for the first time at $z \sim 2$.

Nonetheless, there are several caveats to the current work. First, the MOSDEF survey is slightly biased toward unobscured, star-forming galaxies. This bias, combined with lower success rates for the quiescent (i) and post-starburst (ii) galaxies in the MOSDEF survey, results in a small number of galaxies for these bins. Second, our weighting scheme biases our analysis slightly toward brighter galaxies, as these tend to have higher S/N. This bias primarily affects the bins in which there are few galaxies. Finally, we only consider galaxies with MOSDEF redshifts in this work, so we are biased toward post-starburst and quiescent galaxies with emission lines (from AGN) or bright continuum emission. Future work with NIRSpect on the *James Webb Space Telescope* may overcome these problems without relying on stacking, however such observations at $z \sim 2$ will remain challenging. Such larger and more complete samples would enable the use of number density to longitudinally study the evolution of each bin across redshift.

We would like to thank Dan Kelson for a referee report that improved the clarity and quality of the manuscript. Funding for the MOSDEF survey is provided by NSF-AAG grants AST-1312780, 1312547, 1312764, and 1313171, grant AR-13907 provided by NASA through a grant from the Space Telescope Science Institute, and NASA-ADAP grant NNX16AF54G. This work was performed under the auspices of the U.S. Department of Energy by Lawrence Livermore National Laboratory under Contract DE-AC52-07NA27344. Funding for T.O.Z. was provided by LLNL Livermore Graduate Scholar Program. We also acknowledge the members of the 3D-*HST* collaboration, who provided us with spectroscopic and photometric catalogs used to select MOSDEF targets and derive stellar population parameters.

ORCID iDs

Mariska Kriek  <https://orcid.org/0000-0002-7613-9872>
 Alice E. Shapley  <https://orcid.org/0000-0003-3509-4855>
 Naveen A. Reddy  <https://orcid.org/0000-0001-9687-4973>
 William R. Freeman  <https://orcid.org/0000-0003-3559-5270>
 Brian Siana  <https://orcid.org/0000-0002-4935-9511>
 Alison L. Coil  <https://orcid.org/0000-0002-2583-5894>
 Mojegan Azadi  <https://orcid.org/0000-0001-6004-9728>
 Guillermo Barro  <https://orcid.org/0000-0001-6813-875X>
 Francesca M. Fornasini  <https://orcid.org/0000-0002-9286-9963>
 Gene Leung  <https://orcid.org/0000-0002-9393-6507>
 Sedona H. Price  <https://orcid.org/0000-0002-0108-4176>
 Ryan L. Sanders  <https://orcid.org/0000-0003-4792-9119>
 Irene Shivaiei  <https://orcid.org/0000-0003-4702-7561>

References

- Abramson, L. E., & Morishita, T. 2018, *ApJ*, 858, 40
 Azadi, M., Coil, A. L., Aird, J., et al. 2017, *ApJ*, 835, 27
 Balogh, M. L., Morris, S. L., Yee, H. K. C., Carlberg, R. G., & Ellingson, E. 1999, *ApJ*, 527, 54
 Barden, M., Häußler, B., Peng, C. Y., McIntosh, D. H., & Guo, Y. 2012, *MNRAS*, 422, 449
 Barro, G., Kriek, M., Pérez-González, P. G., et al. 2016, *ApJL*, 827, L32
 Barro, G., Trump, J. R., Koo, D. C., et al. 2014, *ApJ*, 795, 145
 Belli, S., Newman, A. B., & Ellis, R. S. 2015, *ApJ*, 799, 206
 Brammer, G. B., van Dokkum, P. G., & Coppi, P. 2008, *ApJ*, 686, 1503
 Brinchmann, J., Charlot, S., White, S. D. M., et al. 2004, *MNRAS*, 351, 1151
 Bruzual, G., & Charlot, S. 2003, *MNRAS*, 344, 1000
 Calzetti, D., Armus, L., Bohlin, R. C., et al. 2000, *ApJ*, 533, 682
 Chabrier, G. 2003, *PASP*, 115, 763
 Conroy, C., Gunn, J. E., & White, M. 2009, *ApJ*, 699, 486
 Fumagalli, M., Labbé, I., Patel, S. G., et al. 2014, *ApJ*, 796, 35
 Grogin, N. A., Koevski, D. D., Faber, S. M., et al. 2011, *ApJS*, 197, 35
 Kauffmann, G., Heckman, T. M., White, S. D. M., et al. 2003, *MNRAS*, 341, 54
 Khochfar, S., & Silk, J. 2006, *ApJL*, 648, L21
 Koekemoer, A. M., Faber, S. M., Ferguson, H. C., et al. 2011, *ApJS*, 197, 36
 Kriek, M., Conroy, C., van Dokkum, P. G., et al. 2016, *Natur*, 540, 248
 Kriek, M., Shapley, A. E., Reddy, N. A., et al. 2015, *ApJS*, 218, 15
 Kriek, M., van Dokkum, P. G., Labbé, I., et al. 2009, *ApJ*, 700, 221
 Lee, S.-K., Ferguson, H. C., Somerville, R. S., Wiklind, T., & Giavalisco, M. 2010, *ApJ*, 725, 1644
 Lilly, S. J., & Carollo, C. M. 2016, *ApJ*, 833, 1
 Maraston, C., Pforr, J., Renzini, A., et al. 2010, *MNRAS*, 407, 830
 Mendel, J. T., Saglia, R. P., Bender, R., et al. 2015, *ApJL*, 804, L4
 Momcheva, I. G., Brammer, G. B., van Dokkum, P. G., et al. 2016, *ApJS*, 225, 27
 Muzzin, A., Marchesini, D., Stefanon, M., et al. 2013, *ApJ*, 777, 18
 Onodera, M., Renzini, A., Carollo, M., et al. 2012, *ApJ*, 755, 26
 Peng, C. Y., Ho, L. C., Impey, C. D., & Rix, H.-W. 2002, *AJ*, 124, 266
 Poggianti, B. M., Aragón-Salamanca, A., Zaritsky, D., et al. 2009, *ApJ*, 693, 112
 Reddy, N. A., Kriek, M., Shapley, A. E., et al. 2015, *ApJ*, 806, 259
 Reddy, N. A., Pettini, M., Steidel, C. C., et al. 2012, *ApJ*, 754, 25
 Skelton, R. E., Whitaker, K. E., Momcheva, I. G., et al. 2014, *ApJS*, 214, 24
 Spitler, L. R., Straatman, C. M. S., Labbé, I., et al. 2014, *ApJL*, 787, L36
 Tomczak, A. R., Quadri, R. F., Tran, K.-V. H., et al. 2014, *ApJ*, 783, 85
 van de Sande, J., Kriek, M., Franx, M., et al. 2013, *ApJ*, 771, 85
 van der Wel, A., Bell, E. F., Häußler, B., et al. 2012, *ApJS*, 203, 24
 van der Wel, A., Franx, M., van Dokkum, P. G., et al. 2014, *ApJ*, 788, 28
 van Dokkum, P. G., Nelson, E. J., Franx, M., et al. 2015, *ApJ*, 813, 23
 Whitaker, K. E., Kriek, M., van Dokkum, P. G., et al. 2012, *ApJ*, 745, 179
 Whitaker, K. E., Labbé, I., van Dokkum, P. G., et al. 2011, *ApJ*, 735, 86
 Whitaker, K. E., van Dokkum, P. G., Brammer, G., et al. 2013, *ApJL*, 770, L39
 Wild, V., Almaini, O., Dunlop, J., et al. 2016, *MNRAS*, 463, 832
 Williams, R. J., Quadri, R. F., Franx, M., van Dokkum, P., & Labbé, I. 2009, *ApJ*, 691, 1879
 Worthey, G., & Ottaviani, D. L. 1997, *ApJS*, 111, 377
 Wu, P.-F., van der Wel, A., Gallazzi, A., et al. 2018, *ApJ*, 855, 85
 Wuyts, S., Franx, M., Cox, T. J., et al. 2009, *ApJ*, 696, 348
 Yano, M., Kriek, M., van der Wel, A., & Whitaker, K. E. 2016, *ApJL*, 817, L21